Project Sagebrush: Revisiting the Value of the Horizontal Plume Spread Parameter σ_y

D. FINN, K. L. CLAWSON, AND R. M. ECKMAN

Field Research Division, NOAA Air Resources Laboratory, Idaho Falls, Idaho

H. LIU, E. S. RUSSELL, AND Z. GAO

Laboratory for Atmospheric Research, Washington State University, Pullman, Washington

S. BROOKS

University of Tennessee Space Institute, Tullahoma, Tennessee

(Manuscript received 18 September 2015, in final form 18 March 2016)

ABSTRACT

The first phase of an atmospheric tracer experiment program, designated Project Sagebrush, was conducted at the Idaho National Laboratory in October 2013. The purpose was to reevaluate the results of classical field experiments in short-range plume dispersion (e.g., Project Prairie Grass) using the newer technologies that are available for measuring both turbulence levels and tracer concentrations. All releases were conducted during the daytime with atmospheric conditions ranging from neutral to unstable. The key finding was that the values of the horizontal plume spread parameter σ_y tended to be larger, by up to a factor of ~2, than those measured in many previous field studies. The discrepancies tended to increase with downwind distance. The values of the ratio σ_y/σ_θ, where σ_θ is the standard deviation of the horizontal wind direction, also trend near the upper limit or above the range of values determined in earlier studies. There was also evidence to suggest that the value of σ_y began to be independent of σ_θ for σ_θ greater than 18°. It was also found that the commonly accepted range of values for σ_θ in different stability conditions might be limiting, at best, and might possibly be unrealistically low, especially at night in low wind speeds. The results raise questions about the commonly accepted magnitudes of σ_y derived from older studies. These values are used in the parameterization and validation of both older stability-class dispersion models as well as newer models that are based on Taylor's equation and modern PBL theory.

1. Introduction

The horizontal plume spread parameter σ_y and the vertical plume spread parameter σ_z, both derived from Gaussian distributions, are frequently used to model plume dispersion. Early schemes for estimating these parameters were mostly empirical fits to data from tracer experiments. One of the most common of these schemes is the Pasquill–Gifford (P-G) curves (Pasquill 1961), which provide estimates of σ_y and σ_z for six different atmospheric stability classes. More modern models such as "AERMOD" (Cimorelli et al. 2004), the research line source model "RLINE" (Snyder et al. 2013; Venkatram et al. 2013), and the Atmospheric Dispersion Modeling System (ADMS; Carruthers et al. 1994) have moved away from P-G stability classifications and instead estimate the plume spread parameters using a combination of Taylor's (1921) theory and current understanding of the PBL. Nonetheless, these newer schemes remain semiempirical in nature, requiring tracer data to estimate unknown parameters that vary with the scheme.

A small number of short-range tracer experiments conducted in the 1950s and 1960s have been the primary source of data for fitting the empirical components of the σ_y and σ_z schemes. Prominent among these was Project Prairie Grass (PPG; Barad 1958a,b). Other early near-surface experiments include Project Green Glow (Fuquay et al. 1964), Projects Ocean Breeze and Dry Gulch (Haugen and Fuquay 1963), and a series of

Corresponding author address: Dennis Finn, NOAA Air Resources Laboratory, Field Research Division, 1750 Foote Dr., Idaho Falls, ID 83402.
E-mail: dennis.finn@noaa.gov

DOI: 10.1175/JAMC-D-15-0283.1

"uranine" dye releases at the National Reactor Testing Station in Idaho [Islitzer and Dumbauld 1963; the site is now called the Idaho National Laboratory (INL)]. Slade (1968) provides a comprehensive listing of these early tracer experiments together with a summary of the knowledge about dispersion at the time.

PPG remains one of the most-used tracer studies for flat terrain, but it had limitations. The entire study took place during a dry period in Nebraska over a mown grass field during July and August of 1956. Information on vertical dispersion came from a single set of towers 100 m downwind of the source, with a maximum tracer measurement height of 17.5 m AGL. Information on PBL stability and surface fluxes was derived from mean wind and temperature profiles, since no instruments were available at that time for measuring fluxes directly. PPG is still often used as a benchmark for the testing and validation of models, including modern models that are based in PBL theory. Given the limitations of PPG and other classical short-range tracer studies, it is reasonable to raise the question of whether the reported results are repeatable and generally applicable to other regions. Would tracer studies using modern meteorological instrumentation produce results that are similar to those of the classical studies?

In addition to these uncertainties, inspiration for revisiting short-range tracer dispersion comes from a 2008 tracer experiment that the National Oceanic and Atmospheric Administration (NOAA) Air Resources Laboratory Field Research Division (hereinafter ARLFRD) conducted at the U.S. Department of Energy's INL site (Finn et al. 2010). The focus of the 2008 experiment was the effects of roadside sound barriers on vehicle pollution, but a subset of the data was compared with the PPG results and showed interesting deviations (A. Venkatram 2011, personal communication). Were the observed deviations due to different surface roughnesses at the two sites, different methods of measuring boundary layer stability, random variability, seasonal differences, or perhaps something else? Would further tracer-release studies continue to show deviations from the PPG results?

To address some of these uncertainties, ARLFRD planned a series of tracer field studies, designated as Project Sagebrush (PSB). This is a multiple-phase and multiple-year effort to study plume dispersion from continuous sources in the horizontal and vertical directions over a range of seasons, atmospheric stabilities, and wind conditions. The first phase (PSB1) was conducted in October of 2013, and several differences were observed relative to the classical studies and to the dispersion schemes that are based upon those studies. Some of these differences will be detailed here, with others to follow in later papers. A comprehensive report on PSB1, including the rationale and detailed descriptions of the SF_6 tracer and meteorological measurements, can be found in Finn et al. (2015).

This paper will focus on highlighting the differences between PSB1 results and those from past field studies and existing modeling schemes and not on the development of any particular model. The primary purposes of this paper are 1) to provide a summary of Project Sagebrush phase 1, 2) to raise concerns about the representativeness of the σ_y values obtained from PPG for model parameterization and validation, and 3) to raise concerns about the continued widespread usage of the stability-class modeling schemes.

2. Experimental configuration

Project Sagebrush is being executed on the NOAA "Grid 3" tracer dispersion array located on the INL site in southeastern Idaho. The INL is located across a broad, relatively flat plain on the western edge of the Snake River Plain (SRP) in southeastern Idaho. Elevations across the INL are approximately 1500 m MSL. Several parallel mountain chains with peaks exceeding 3000 m MSL dominate the western edge of the SRP. These chains are separated by a series of tributary valleys that feed into the SRP. The mountains and benches forming the eastern side of the plain are somewhat lower in elevation, with mountain peaks at roughly 2200 m MSL. Several tributary valleys also feed into the plain from the east, but they are not as regularly spaced as those to the west.

The Grid 3 area (Fig. 1) was specifically designed to conduct tracer dispersion studies, and numerous studies have been conducted there over time (e.g., Start et al. 1984; Sagendorf and Dickson 1974; Garodz and Clawson 1991, 1993a,b; Finn et al. 2010). Conducting PSB at Grid 3 also allows ARLFRD to include valuable knowledge from previous work gained over the years as well as to make use of all of the meteorological measurements from a large meteorological tower network in the region (Clawson et al. 2007; Rich et al. 2015, manuscript submitted to *J. Idaho Acad. Sci.*).

A notable element of the network is a 62-m tower (designated as GRI) at Grid 3 that provided vertical profiles of wind, turbulence, fluxes, and air temperature. Analyses of data from this tower showed that the near-surface wind usually blows parallel to the axis of the SRP, with southwest winds common during the day and northeast winds at night (Clawson et al. 2007). GRI lies about 13 km southeast from the nearest mountains, but the orientation of the prevailing winds means that the tracer facility has a relatively flat, uniform fetch extending many tens of kilometers in the prevailing upwind direction. The boundary

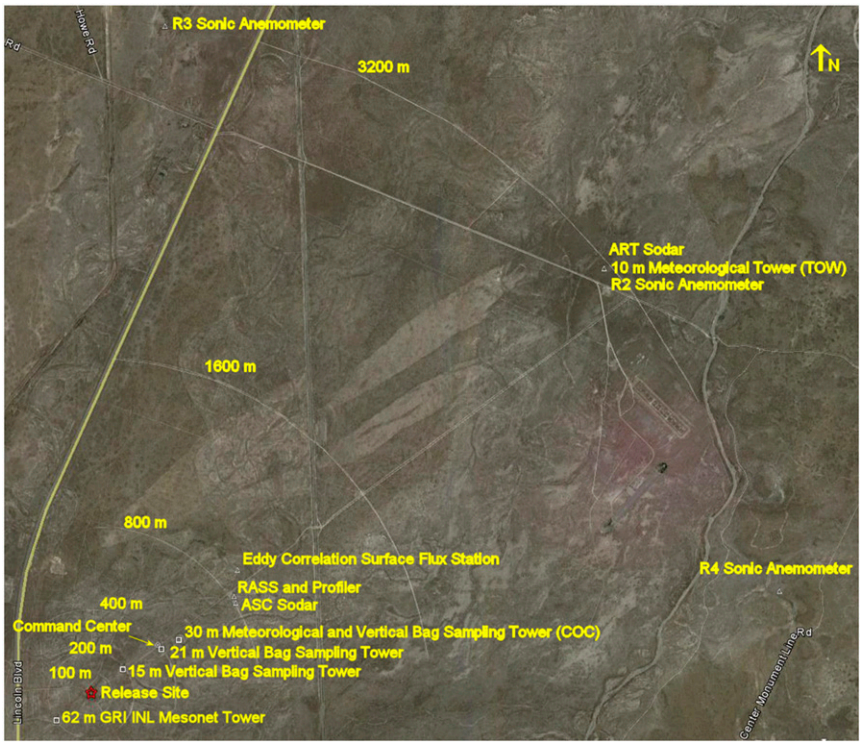

FIG. 1. Image of the experimental field site showing tracer bag-sampling arcs, northeastern axial road, and locations of some key sites (image is copyright by Google, Inc.).

layer under such conditions is expected to be mostly uniform.

The site also offers relatively uniform aerodynamic characteristics across the Grid 3 area (Fig. 2). The canopy is mostly sagebrush and grass. GRI has routine wind and temperature measurements at 2, 10, 15, 45, and 60 m above the ground. Wind profiles from this tower in near-neutral conditions have been used in a statistical algorithm to estimate the roughness length z_0 at the tracer facility. For the southwesterly winds that are common during the day, the median z_0 is 3 cm, with a 90% probability interval of 2.5–3.5 cm. For the northeasterly winds that are common at night, the median z_0 is 3.8 cm, with a 90% probability interval of 3.3–4.4 cm. The slightly higher roughness length for northeast winds may be due to the old river channels and low terrain undulations to the north of the facility. Estimates of the displacement height d were also computed from the GRI profiles, but the values are not significantly different from zero. A small displacement height of a few centimeters probably exists but is not detectable with the current observations on the tower.

During PSB1, a twin-engine Piper Navajo aircraft operated by the University of Tennessee Space Institute was available for making fast-response airborne SF_6 measurements. Because of minimum altitude restrictions and the need to operate the aircraft in daylight, the PSB1 tracer releases were limited to unstable and neutral conditions. These airborne measurements will not be described further here, but the presence of the aircraft explains the lack of releases in nighttime stable conditions during phase 1.

Five SF_6 tracer releases took place from 2 to 18 October 2013. Because the releases were restricted to the daytime when prevailing winds are from the southwest, the study domain was located primarily on the northeast quadrant of the Grid 3 tracer dispersion array (Fig. 3). Twenty-eight bag samplers were placed at 3° intervals from 4° azimuth to 85° azimuth along each of the four circular arcs designated for a test. These were either the 200-, 400-, 800-, and 1600-m arcs or the 400-, 800-, 1600-, and 3200-m arcs, depending upon the forecast PBL stability and the planned release rate. Each bag sampler was mounted at 1 m AGL and contained 12 bags. The SF_6 tracer was released continuously at a constant rate from a point source at 1.5 m AGL at the center of the dispersion array for each test. The releases began 0.5 h prior to the start of sampling on the dispersion array to establish a quasi–steady state SF_6 plume across all of the arcs. The release then continued at a constant rate for the 2-h duration of the sampling in the test. The 12 bags collected samples sequentially, with each bag covering a 10-min interval, and therefore concentration averaging

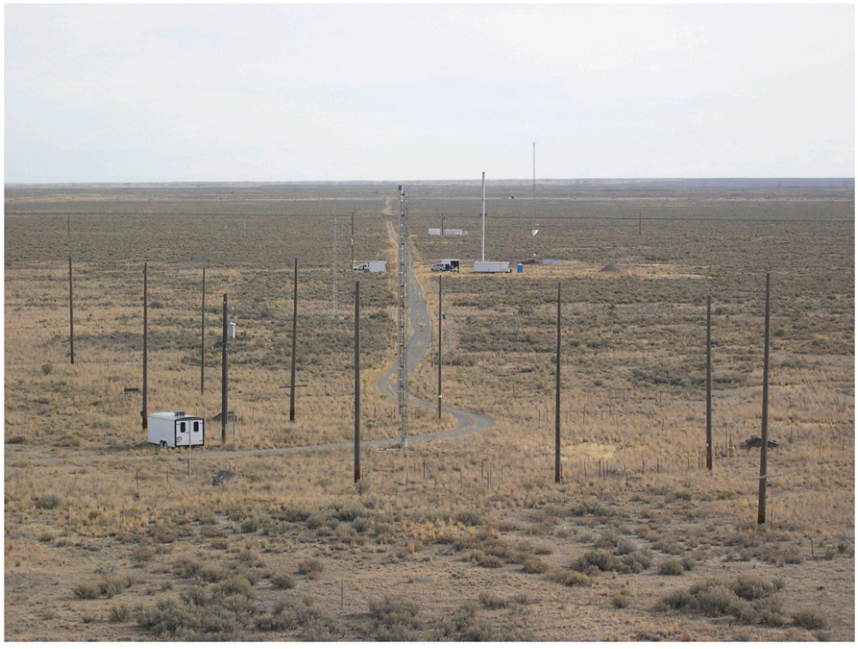

FIG. 2. Looking northeast from the Grid 3 tower (GRI) along the axial road at 55° azimuth across the sampling array. The release point was located at the tall tower closest to the camera.

times between 10 min and 2 h are available at each location. Release rates were set upon the basis of preliminary calculated estimates of concentrations at different heights and distances, the anticipated atmospheric stability conditions, and whether the aircraft would be making tracer measurements during a test. Full details of the tracer bag sampling, analyses, and release can be found in Finn et al. (2015).

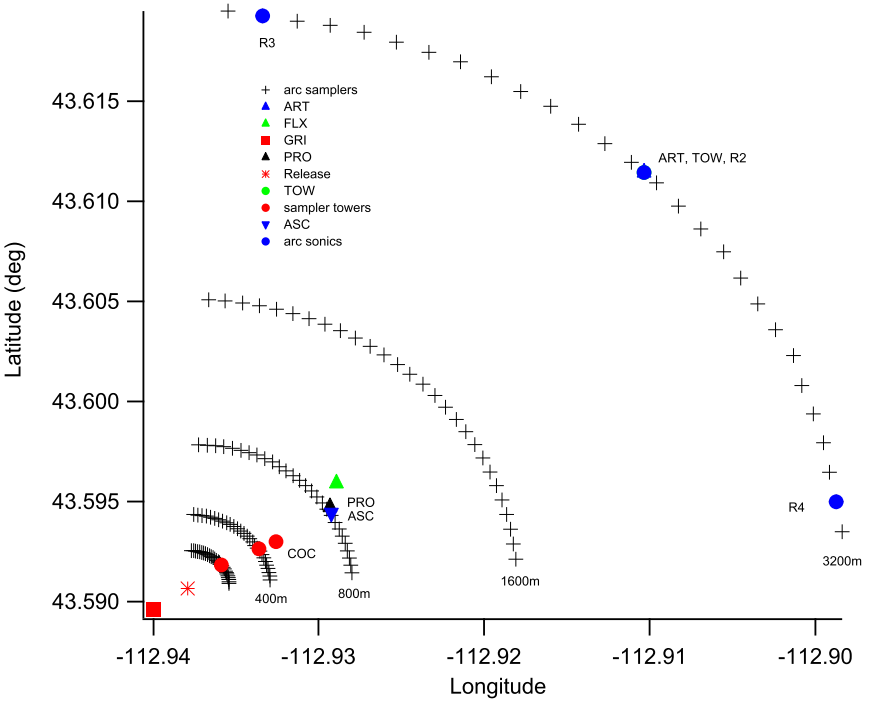

FIG. 3. Schematic representation of the NOAA Grid 3 field-study site showing the locations of the bag samplers on arcs, release point, towers, and meteorological measurement sites.

TABLE 1. Test summaries. The superscript plus sign after the date denotes aircraft sampling. Start times are in mountain standard time. The friction velocity u_* (m s^{-1}) and Obukhov length L (m) represent the average of the four half-hour calculations, using two-axis rotation, that cover the sampling periods at sonic anemometers R3 and R4 on the 3200-m arc. The mixing height z_i (m) is the average of the before and after estimates as based on potential temperature from the radiosonde soundings.

Test	Date	Start time	Release rate (g s^{-1})	Meteorological summary	R3 u_*	R4 u_*	R3 L	R4 L	z_i
1	2 Oct 2013$^+$	1430	10.177	Mostly sunny with cirrostratus haze. Wind speeds 1–2 m s^{-1}; σ_θ 18–67°	0.12	0.17	−4.1	−13.7	1115
2	5 Oct 2013$^+$	1300	9.986	Mostly sunny. Wind speeds 2.4–4.8 m s^{-1}; σ_θ 10–64°	0.22	0.24	−5.5	−8.0	1137
3	7 Oct 2013$^+$	1300	9.930	Mostly sunny. Wind speeds 7.3–10.0 m s^{-1}; σ_θ 8–11.5°	0.59	0.55	−109.7	−93.6	951
4	11 Oct 2013	1400	1.043	Mostly sunny. Wind speeds 4.3–5.9 m s^{-1}; σ_θ 9.5–20°	0.37	0.31	−24.6	−17.0	2131
5	18 Oct 2013	1300	1.030	Mostly sunny. Wind speeds 3.6–5.0 m s^{-1}; σ_θ 11–22°	0.36	0.33	−21.2	−17.5	1129

Three towers, all visible in Figs. 1 and 2, were available for vertical tracer sampling to the northeast of the source. The first of these was 15 m (50 ft) tall and was located at the intersection between the 55° azimuth radial road and the 200-m arc. Samplers were mounted at 1, 5, 10, and 15 m AGL on this tower. The second tower was 21 m tall and was located at the intersection of the radial road and the 400-m arc. Samplers were mounted at 1, 5, 10, 15, and 20 m AGL on this tower. The third tower was 30 m tall (100 ft) and was located 499 m from the source at ~60° azimuth. This tower served a dual purpose as the meteorological tower for the nearby command center (COC). Samplers were mounted at 1, 5, 10, 15, 20, 25, and 30 m on this tower.

In addition to the bag samplers, six fast-response SF_6 analyzers were deployed during PSB1 to measure concentration fluctuations (Finn et al. 2015). Five of these were mounted in vehicles and collocated with a bag-sampling location on the sampling arcs. One analyzer was mounted in the airplane during tests 1, 2, and 3. During tests 4 and 5, the airplane was not available and this analyzer was relocated to a fixed site on the sampling arcs. The fast-response data will have only brief mention here.

Every effort was made to characterize fully the conditions and structure of the boundary layer for the purpose of identifying all possible meteorological factors controlling tracer dispersion (Finn et al. 2015). To this end, ARLFRD, in collaboration with the Laboratory for Atmospheric Research at Washington State University (WSU), deployed a broad array of meteorological instrumentation and measurements as indicated in Fig. 3:

1) the 62-m Grid 3 GRI tower, with cup and vane anemometers at five levels (2, 10, 15, 45, and 60 m), 3D sonic anemometers at seven levels (from ARLFRD at 4, 30, and 45 m and from WSU at 2, 8, 16, and 60 m), 2D sonic anemometers at six levels, air temperature and RH at 14 levels, infrared gas analyzers at four levels, solar radiation at one level, barometric pressure at three levels, net radiometers at two levels, an infrared radiometer, soil heat flux at two levels (WSU), and soil moisture and temperature at five levels (ARLFRD),
2) three 3D sonic anemometers arrayed along the 3200-m arc (R2, R3, and R4),
3) the 30-m COC meteorological tower, with cup and vane anemometers at three levels,
4) a 10-m meteorological tower at 3200 m (TOW), with cup and vane anemometers at two levels,
5) sodars at 800 (ASC) and 3200 (ART) m (wind profiles from 30 to 200 m),
6) 915-MHz radar wind profiler (PRO) and RASS at ~800 m (winds up to 2.9-km height and temperatures up to ~1-km height),
7) radiosonde launches before and after each test,
8) eddy-correlation surface flux station at about 900 m on the dispersion array (FLX), with 3D sonic anemometer, infrared gas analyzer, solar radiation, net radiometer, air temperature/relative humidity, barometric pressure, soil temperature at two levels, soil moisture, and soil heat flux at four locations, and
9) 33 other (in addition to GRI) meteorological stations of the NOAA/INL mesonet.

A brief summary of test dates and times, release rates, meteorological conditions, and atmospheric stability is given in Table 1.

3. Results for plume spread parameter σ_y

a. Plume cross-sectional characteristics

PSB1 plume cross sections tended to exhibit complex internal structure with significant variability, at least on

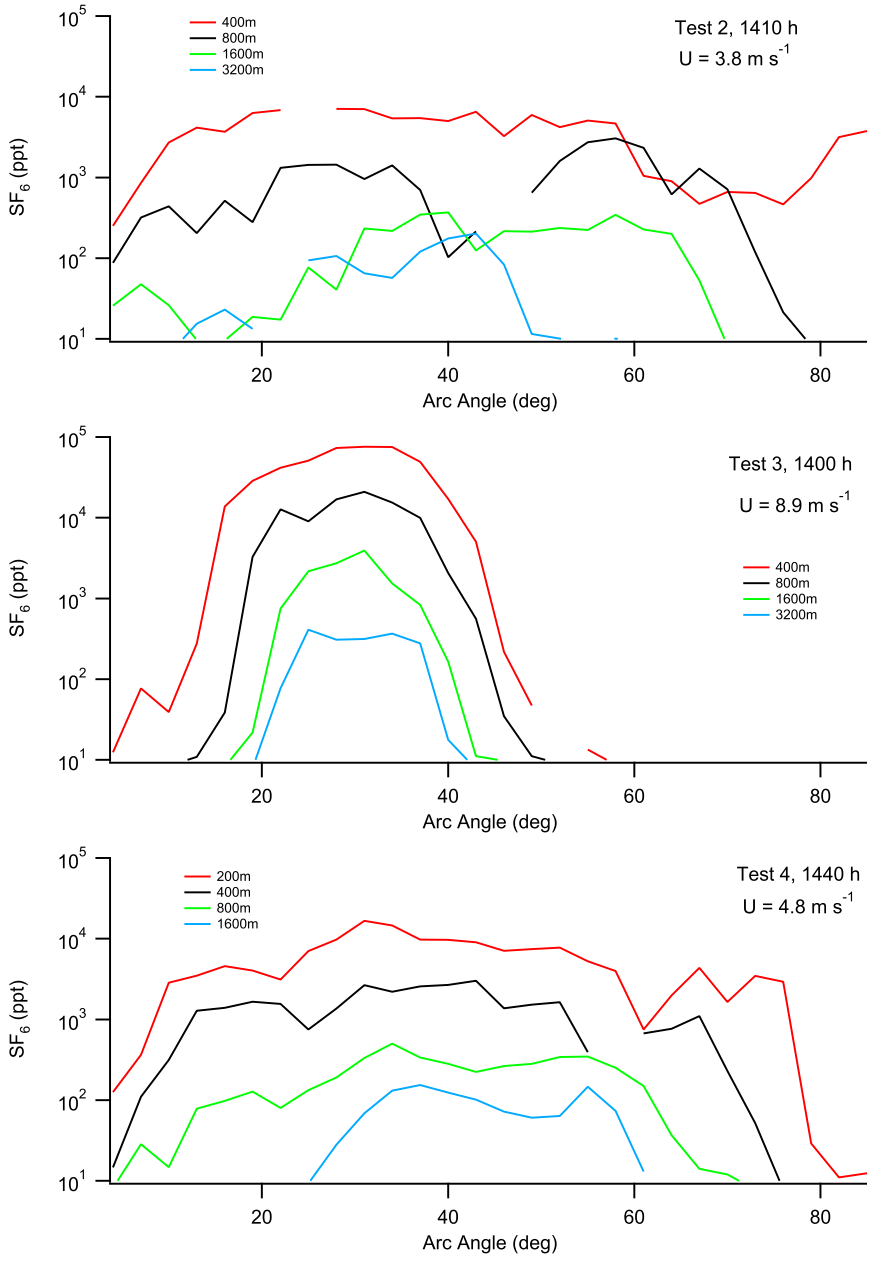

FIG. 4. Examples of plume cross-sectional profiles from tests 2, 3, and 4. Times and wind speed U are shown in the annotation, and distances are indicated in the legends. The cross sections all represent 10-min-average concentrations.

the basis of 10-min sample averaging. Cross sections deviated considerably from an idealized Gaussian form, with a few exceptions that occurred mostly during test 3. Some examples are shown in Fig. 4. Large, irregular concentration variations, distinct outlier peaks that are separate from the main plume, and skewed asymmetry of concentrations around the peak concentration for individual cross sections were all very common. Furthermore, some of the cross sections exhibited truncated profiles at the edge of the sampling array. Truncated profiles will be defined as those in which the concentration at an end arc position was greater than 10% of the maximum concentration along the arc. Some typical PPG examples (data are from http://envs.au.dk/en/knowledge/air/models/background/omlprairie/excelprairie/) are shown for comparison in Fig. 5. It can be seen that the PPG plumes have much narrower arcs than the PSB1 plumes for comparable wind speeds and downwind distances.

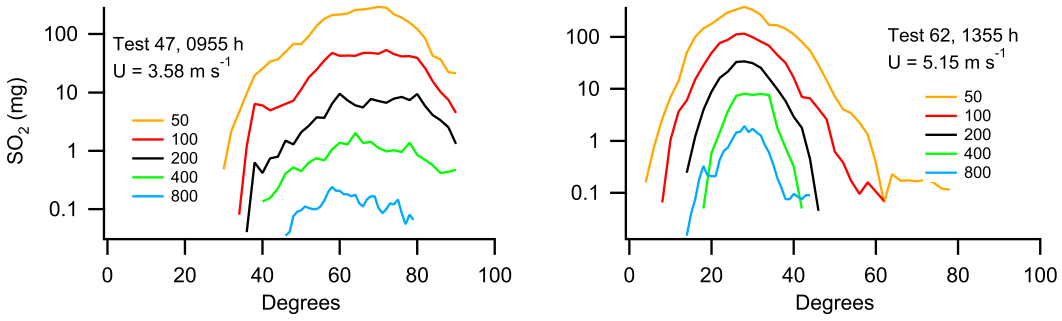

FIG. 5. Example PPG plume cross sections, with times and wind speed U shown in the annotation and distances indicated in the legends. The cross sections represent 10-min integrated sampling concentrations.

b. *Methods used for determining* σ_y

Three approaches were used to estimate the horizontal plume spread parameter σ_y, with the first two using PSB1 tracer data. The first was based on crosswind integration along the sampling arc to determine the second moment about the mean of the data. The plume width was estimated by calculating the second moment about the mean of the data:

$$\langle Y\rangle^2 = \frac{1}{A}\int_{-\infty}^{\infty}(Y - Y_0)^2 C\,dy,$$

where Y is the cross-plume coordinate in meters, C is the concentration (ppt) as a function of cross-plume distance, Y_0 is the weighted plume centerline, and A is the integrated concentration, such that

$$Y_0 = \frac{1}{A}\int_{-\infty}^{\infty} YC\,dy \quad \text{and}$$
$$A = \int_{-\infty}^{\infty} C\,dy;$$

σ_y was then calculated as the square root of $\langle Y\rangle^2$.

A second method used Gifford's (1961) relationship

$$\sigma_y = x\tan(W/2)/2.15,$$

where x is the downwind distance in meters and W is the plume width in radians at the points where the concentration values decrease to 10% of their centerline magnitude. This method assumes a Gaussian distribution of the plume.

The third approach was based on the relationship between plume spread and the value of σ_θ, the standard deviation in wind direction in radians, with $\sigma_y = x\sigma_\theta$ in the near field (Taylor 1921; Pasquill 1961). It was used to check the results of the two methods. An empirical exponent for the downwind distance x, usually ranging in value from 0.85 to 0.894 (Cramer et al. 1964; Martin 1976; Eckman 1994), is used to account for the increase in wind speed with height in some dispersion schemes ($\sigma_y = x^b\sigma_\theta$). Lower values of b have been proposed for a restricted range of σ_θ (Cramer et al. 1964; Slade 1968).

The concentration variability noted in section 3a introduced complications and significant uncertainties with respect to the use of the first two methods described above that are due to the implied assumptions of Gaussian behavior. Determination of the plume centerlines and maximum concentrations was particularly uncertain. Furthermore, neither the second-moment method nor the Gifford method was optimal for dealing with plume truncation at the edge of the sampling array.

c. *Method comparison using the average of aligned and combined plume cross sections*

To partially account for the non-Gaussian behavior with 10-min averaging and plume meander, the individual 10-min profiles for tests 2–5 were shifted such that the approximate centroid of each cross section was aligned with the others and then the 12 cross sections over the 2-h release were averaged. The approximate centroid for each plume cross section was determined by computing the first moment Y_0. Although this exercise involved combining cross sections representing somewhat different stabilities over the two hours, it generated plumes that, in general, came much closer to the idealized Gaussian form. This was not done for test 1 because of the very large plume spread and the limited time during which the plume was over the sampling array.

A comparison of the three approaches is shown in Fig. 6. The value of b was set to 1.0 and 0.894 in this comparison. The results for the third method are strongly sensitive to the value of b. Most of the curves lie near the 1:1 line, showing good agreement among the methods. There are discrepancies for test 3 in which the second-moment method provides larger estimates of σ_y except for $b = 1.0$. The estimates of σ_y determined by the $x^b\sigma_\theta$ method are biased in the low direction in test 5 and very much in the high direction for test 2 for $b = 1.0$.

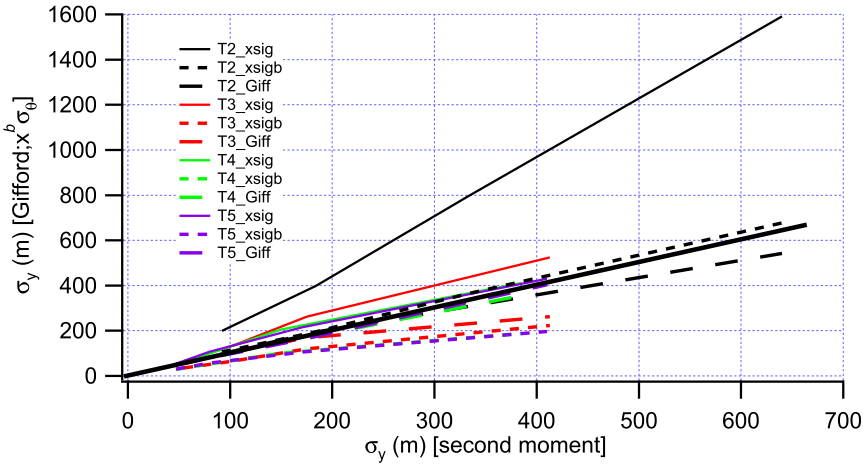

FIG. 6. Comparisons of σ_y calculated by the three methods using shifted, aligned, and combined plume cross sections for tests ("T") 2, 3, 4, and 5. For "xsig" the value of $b = 1.0$; for "xsigb" the value of $b = 0.894$. The thick line is a 1:1 reference.

d. Comparisons with classical studies

The value of σ_y strongly depends on PBL stability, which is one reason why the original P-G curves are split into the six stability classes ranging from A (highly unstable) to F (highly stable). Although modern dispersion approaches model turbulent mixing as a continuum, the A–F stability classification was the original method used to summarize the results of the classical tracer studies. Moreover, this simple classification scheme remains in widespread use, particularly in rapid-response and screening models such as the Areal Locations of Hazardous Atmospheres model (ALOHA; Jones et al. 2013); "HotSpot" (Homann and Aluzzi 2014), and the Clean Air Act Assessment Package—1988 (CAP88; Trinity Engineering Associates 2013). For these reasons, it is still instructive to compare the PSB1 results with various σ_y curves that have been generated from the old studies. At a minimum, such a comparison provides useful information about the repeatability of the tracer results.

For analyzing the PSB1 results, the Pasquill stability class was determined using the U.S. Environmental Protection Agency (EPA) σ_θ method (EPA 2000). Use of the Solar Radiation-Delta T method (SRDT; EPA 2000) was also investigated, but it limited the results to a narrow range of stabilities. One set of curves used for comparison with PSB1 is the original Pasquill–Gifford curves (Pasquill 1961; Gifford 1961). The P-G curves were later refined (Turner 1970; Martin 1976; Pasquill 1976), and additional dispersion schemes utilizing the A–F stability classification were introduced. The Markee (Sagendorf et al. 2001; Start and Wendell 1974; Fuquay et al. 1964) and Briggs (Briggs 1974; Gifford 1976) curves are also included here in the comparisons.

Since the PSB1 bag samplers collected 10-min-average concentrations sequentially over the two hours of each release, the effects of concentration averaging time can also be evaluated. Ideally, the plume edges should be bounded by background level concentrations of ~8 ppt SF_6 on both ends of an arc, but this was often not the case. Therefore, truncated concentration profiles were excluded from the σ_y second-moment calculation. Then, the effects of averaging time were examined using all nontruncated 10-min cross sections. The 10-min bag samples were averaged over 20-, 30-, 40-, and 60-min periods for successive periods not interrupted by truncated cross sections. The averaging was done by arc position, with no plume realignment.

The PSB1 measurements of σ_y, calculated using the second-moment method and classified by Pasquill stability class and averaging period, are shown in Fig. 7. They are compared with those determined from the P-G, Markee, and Briggs dispersion-model curves. One salient feature is that the calculated PSB1 σ_y results are, with the exception of class A, consistently high by a factor of ~2 relative to the published dispersion curves shown. Also shown in Fig. 7 are the σ_y obtained using the second-moment method for the tracer data from PPG classified by the EPA σ_θ method. There was only one case of class A and one case of class B during PPG based upon the EPA σ_θ method. There is good agreement between the PPG data and the model curves out to the extent of the PPG data at 800 m. The PSB1 data are somewhat consistent with the model curves out to 400 m, but beyond that the PSB1 σ_y values begin to deviate considerably, except for class A.

Another feature of Fig. 7 is that the effect of the averaging time on the PSB1 σ_y values is surprisingly small.

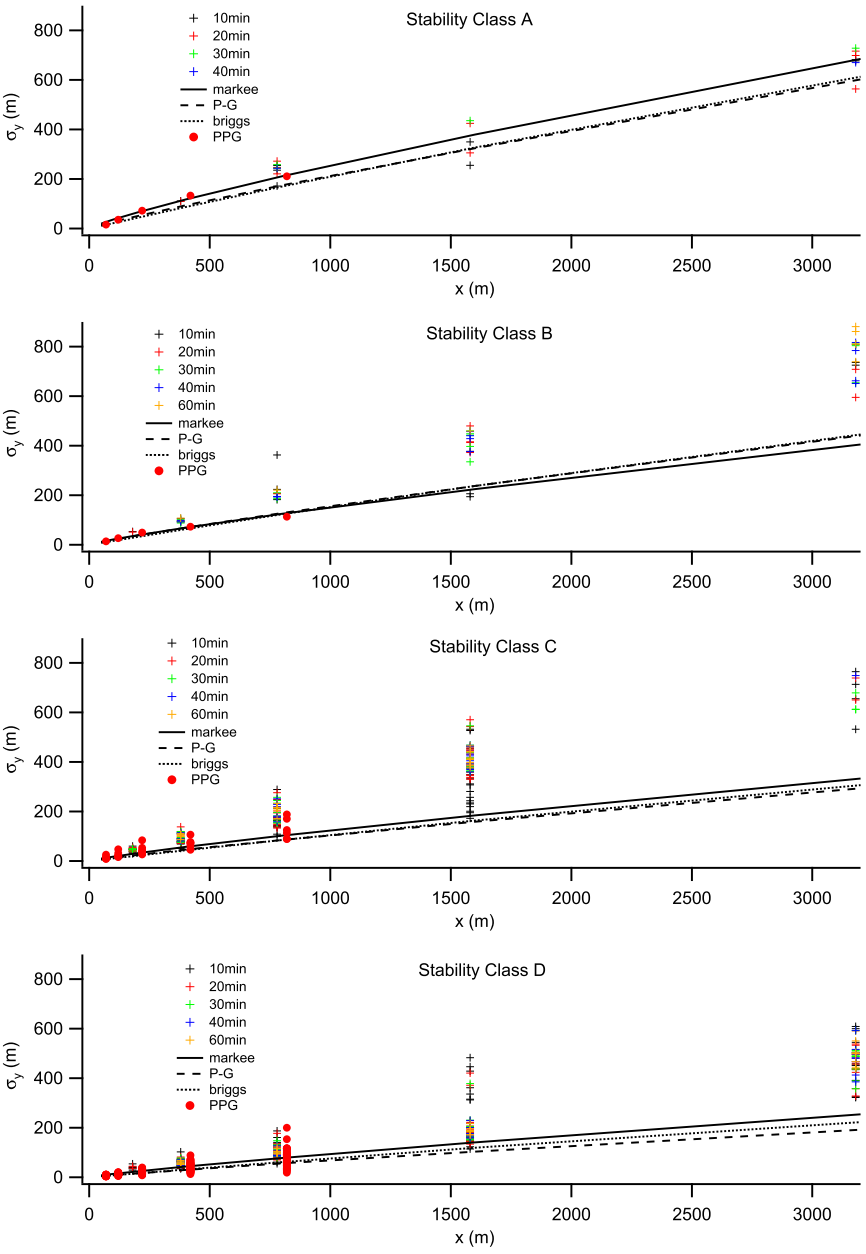

FIG. 7. Estimates of σ_y using the second-moment method for stability categories A–D and averaging periods ranging from 10 to 60 min. The corresponding estimates of σ_y determined by the Markee, P-G, and Briggs dispersion schemes for each A–D stability category are shown for comparison. Also shown are the σ_y from PPG for each stability class. PSB1 data points are shifted by −20 m and PPG data are shifted by +20 m along the x axis to avoid overlaps.

If large scatter is discounted, there is a suggestion of a trend toward higher values of σ_y as averaging time increases, but it is not obvious. Larger values of σ_y would be anticipated for longer averaging times as the effects of lower-frequency wind meander are more fully incorporated into longer averaging periods. Some previous work has found that σ_θ was a function of sampling time and surface roughness and increased by a factor of 2 for 1-h averaging relative to 3-min averaging (Pasquill 1975, 1976). A common adjustment that has been used in the past is a 0.2 power law for averaging time.

One issue to consider in evaluating the results is that the method of averaging is different between PSB1 and the classical studies. In the earlier studies, the tracer

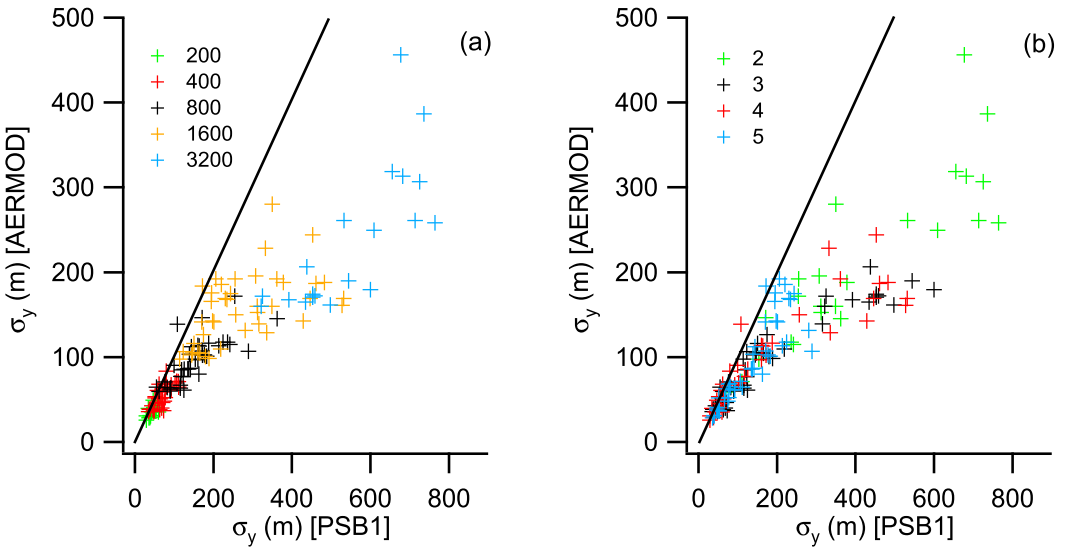

FIG. 8. Plots of 10-min-period σ_y predicted by AERMOD vs those estimated from PSB1 data using the second-moment method, in terms of (a) downwind distance x and (b) test number. The black lines are 1:1 references.

samplers were operated continuously while the averaging time was set by shutting off the source after a specified time interval. In other words, these studies were looking at elongated puffs resulting from a limited release period. In PSB1, the tracer was released continuously over a period exceeding 2 h. The averaging time was set by programming the bag samplers to sequentially switch to a new bag every 10 min. Sampling a continuous plume for 10 min is not necessarily equivalent to sampling a release of 10-min duration. In the former case, the tracer being sampled in any given 10-min interval may have been released from the source over a period well in excess of 10 min. Because of the different release configuration, the effects of averaging time in the PSB1 observations may differ from previous studies. The fast-response analyzer data indicated that plume-meander periodicities were commonly on the order of 12–15 min or less.

Figure 8 shows a comparison between the σ_y predictions of AERMOD (Cimorelli et al. 2004), a model that uses more recent PBL theory to estimate turbulence levels, and results from PSB1. The equation used in AERMOD is

$$\sigma_y = \frac{\sigma_v x}{U}\left(1 + \alpha\frac{\sigma_v x}{U z_i}\right)^{-p},$$

in which z_i is the PBL depth, U is wind speed, σ_v is the crosswind standard deviation in wind speed, and α and p are empirical constants. This semiempirical scheme is based on the near- and far-field limits of Taylor's (1921) equation and assumes that the time scale that determines the transition to the far-field limit scales with z_i/σ_v. The values of the empirical constants were found to be $\alpha = 78$ and $p = 0.3$ on the basis of fits to PPG data. In Fig. 8 the value of z_i was taken as the estimated height of the boundary layer based on radiosonde potential temperature profiles before and after the tracer releases. The values of σ_v and U from the 4-m level on GRI were used in the calculations. It is clear from Fig. 8 that the α and p values, as derived from PPG, do not fit the PSB1 results.

It is worth noting that if there were no edge effects on the tracer sampling, the result would be still larger σ_y. There were numerous profiles included in the determinations of σ_y for which the tracer concentrations were greater than background levels of ~8 ppt SF_6 at one or both ends of the arc but less than 10% of the maximum concentration along the profile. While concentrations in this range tended to be skewed toward background concentrations, the criterion of less than 10% of maximum would still have the effect of somewhat reducing the magnitude of σ_y calculated for these profiles as a result of exclusion of some portions of the tail(s).

e. *PSB1 measurements of σ_θ and turbulence intensity*

The range of σ_θ measured during PSB1 is summarized in Fig. 9 as a function of wind speed. PSB1 σ_θ were calculated from wind vanes in Campbell Scientific, Inc., CR23X dataloggers using the Yamartino method (Yamartino 1984) with 1-s sampling and 5-min averaging periods. The 5-min periods were then averaged to 10-min periods on the basis of the procedure given in EPA (2000). Figure 9 also shows the observed values of

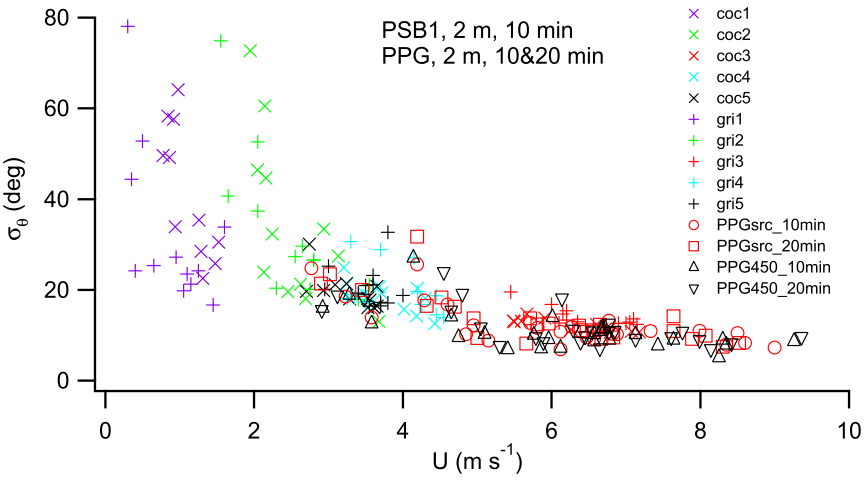

FIG. 9. Ten-minute-average wind vane σ_θ for all tests from COC and GRI at 2 m AGL as a function of cup anemometer wind speed. The test number (1–5) is appended to the COC or GRI designation. The 10- and 20-min-average daytime PPG results at the source (src) and 450 m downwind are shown for comparison.

σ_θ from PPG. There is no evidence in this figure to suggest that the daytime values of σ_θ in PBS1 differ in a systematic way from those in PPG.

The cup anemometers and wind vanes on the GRI, COC, and TOW towers gave generally consistent results for wind speed, wind direction, and σ_θ across the study area (Finn et al. 2015). The σ_θ results for tests 2, 3, and 4 are representative of the range of values observed during PSB1 (Fig. 10). Although spatial variation in σ_θ was sometimes observed across the study area, the overall tendency was toward horizontal homogeneity.

Vertical profiles from GRI of σ_θ, measured by wind vane, and turbulence intensity (σ_v/U), measured by sonic anemometer, are shown in Fig. 11. The wind vane results have been converted to radians for the purpose of comparison with the turbulence intensities. The ranges of turbulence intensities measured by the sonic anemometers during PSB1 were consistent with the σ_θ measured by wind vane. The kinks in some of the sonic profiles are mostly due to transitions between WSU and ARLFRD sonic anemometers. Each WSU sonic anemometer was collocated with an infrared gas analyzer (IRGA). It is suspected that the proximity of the IRGAs might have contributed to the larger values often associated with the WSU sonic anemometers relative to the ARLFRD sonic anemometers (no IRGA).The fact that there were three makes of sonic anemometer involved could also be a factor (Campbell Scientific model CSAT3 at 2, 8, 16, and 60 m; Gill Instruments, Ltd., models R3 and Windmaster Pro at 4 and 30 m, and R.M. Young Co. model 81000 at 45 m).

There was no evidence of anemometer instrumentation problems during PSB1 or that the σ_θ measurements were flawed or anomalous. The wind vane results in Fig. 10 exhibit internal consistency. The sonic anemometer measurements of wind speed, wind direction, and turbulence on GRI and along the 3200-m arc (TOW; sonic anemometers R2, R3, R4) were consistent with other measurements at comparable heights and provided evidence of horizontal homogeneity. The cup anemometers and wind vanes are modern instruments that had been checked and calibrated to modern standards days prior to the experiments. The sonic anemometer measurements of turbulence intensity provide an independent check on the wind vane measurements of σ_θ as well as independent checks between the WSU and ARLFRD sonic anemometers (Fig. 11). There were some differences, but the overall ranges and magnitudes were consistent among the cup anemometers and wind vanes, WSU sonic anemometers, and ARLFRD sonic anemometers.

Although a greater fraction of the σ_θ measurements during PSB1 fell within the more unstable P-G stability classifications than was observed during the daytime PPG experiments, as determined by the EPA method, the overall range of variation in σ_θ was similar for PSB1 and PPG. Figure 12 shows there was no discernible difference in daytime measurements between σ_θ determined by both sonic anemometer and wind vane measurements during autumn 2013 at the INL test site and those from PPG. Here, wind vane values of σ_θ have been converted to radians to facilitate comparisons with sonic anemometer measurements of turbulence intensity. The PPG results shown here are for the PPG wind vane near the source using 10-min averaging. Results from the wind vane at 450 m during PPG were closely comparable to it, as are the results using a 20-min averaging period (Fig. 9).

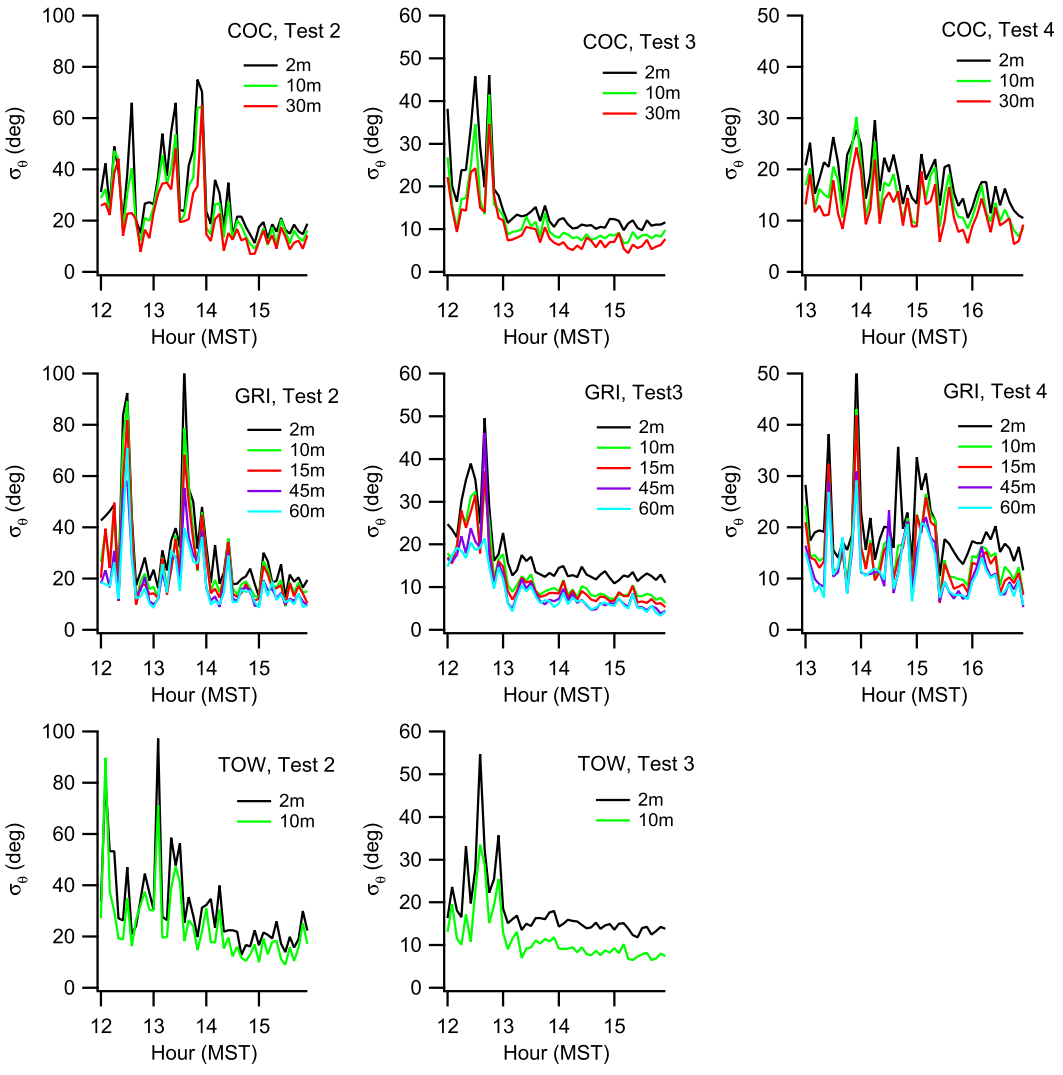

FIG. 10. Wind vane measurements of σ_θ during tests 2, 3, and 4 during PSB1.

Given the importance of the direct physical relationship between σ_θ and σ_y, this line of inquiry prompted an investigation into nighttime measurements of σ_θ. These present a much different picture. The nighttime PPG values of σ_θ are biased in the low direction with respect to a suite of measurements from autumn 2013 at the INL site (Fig. 12). The nighttime bias is most apparent at lower wind speeds. Even when the PPG mean is similar in value to others in their respective wind speed bin, they better match σ_θ measured at higher heights. Furthermore, the range of variability is severely constricted relative to the INL measurements. The daytime and nighttime measurements reported in Fig. 12 are for the hours 1000–1600 and 2200–0400 mountain standard time, respectively. It is beyond the scope of this paper, but it was found there were daytime and nighttime differences for σ_θ between PPG and a suite of other sites and not just the INL site.

The source of the differences between PPG and other sites is not clear. One possible contributor is the wind direction sampling rate. Wind directions were sampled every 2.5 s during the PPG experiments. The cup and vane instrumentation was sampled every second during PSB1, and the sonic anemometers sampled at 10 Hz. Some of the variability in wind direction might not be captured at a lower sampling rate. The PPG anemometers might have had different response characteristics, but that still leaves the question as to why there is a difference between day and night.

f. *Relationship of σ_y to σ_θ*

Figure 13 shows calculated PSB1 σ_y as a function of σ_θ for different distances and averaging periods. There is a suggestion of a linear dependence of σ_y on σ_θ for values of σ_θ up to 18°. The value of σ_y appears to be independent of

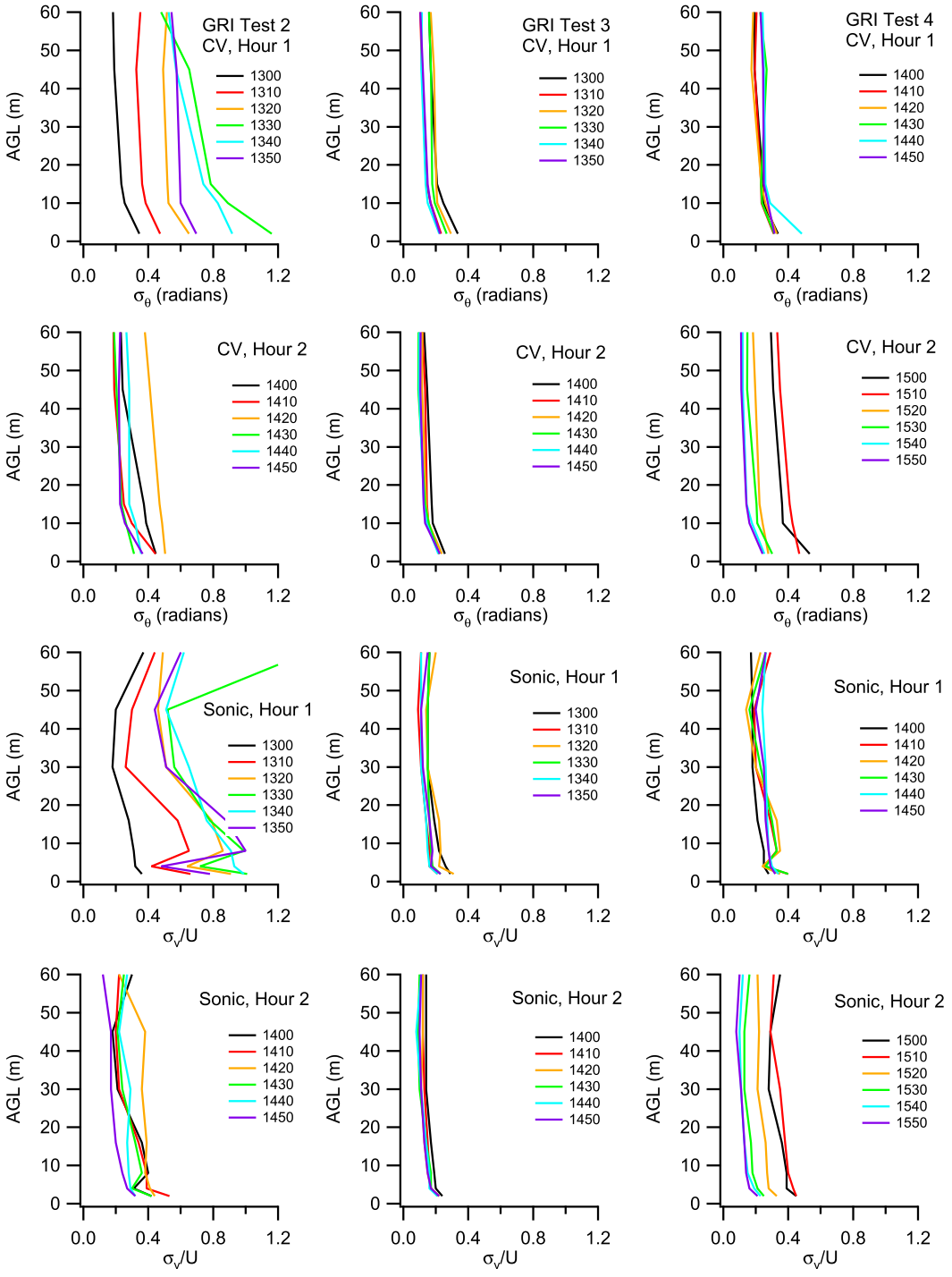

FIG. 11. Comparisons between GRI wind vane ("CV") σ_θ measurements, converted to radians, and sonic anemometer measurements of turbulence intensity for each 10-min period of tests 2, 3, and 4. Times indicated in the legends are start times in mountain standard time.

σ_θ for values greater than ~18°. Of course, the relation between σ_y and σ_θ from Taylor's equation is based on a small-angle approximation, and therefore it becomes invalid at large values of σ_θ. Moreover, the Gaussian plume model requires the slender-plume approximation (Arya 1999), which also is invalid at large σ_θ.

As discussed in section 3d, the σ_y measured during PSB1 are larger than those found in many of the field studies

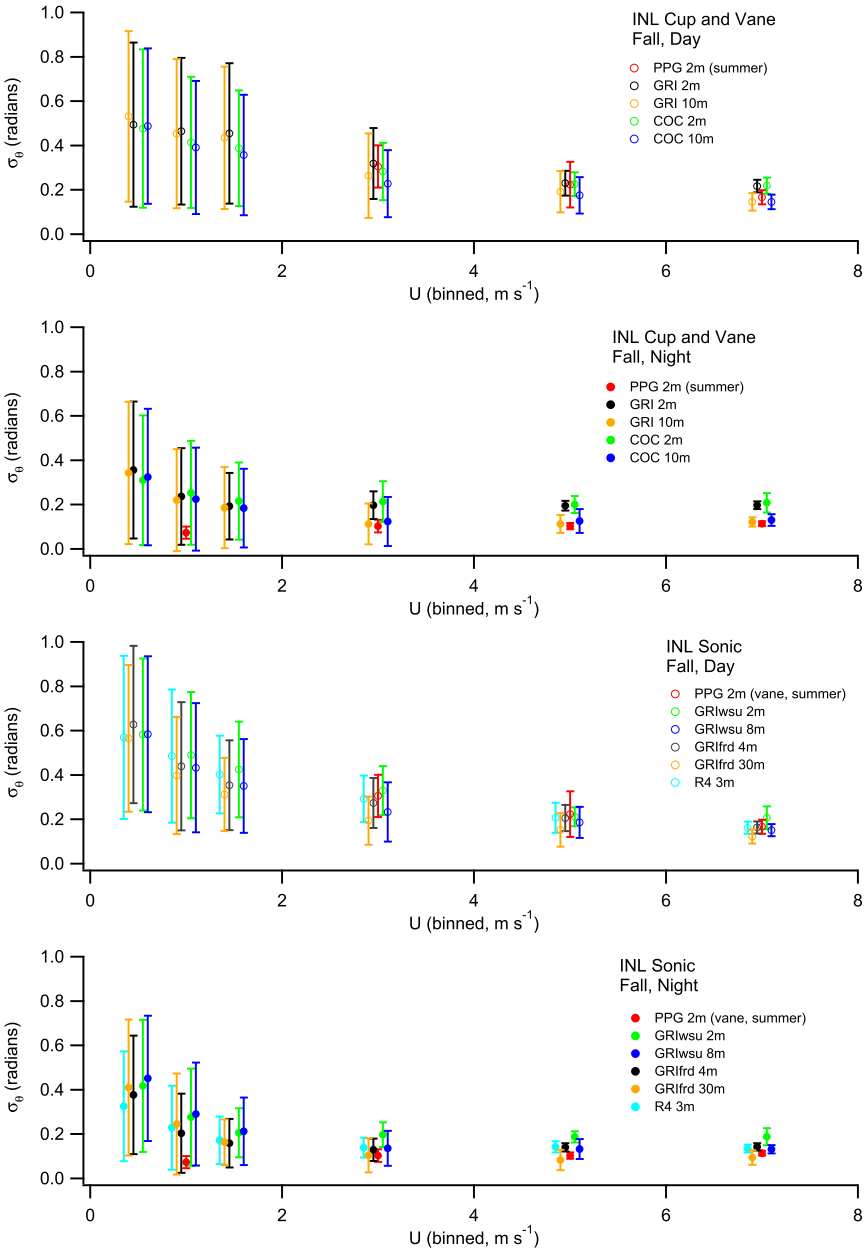

FIG. 12. Ten-minute-average σ_θ expressed in radians for wind vane and sonic anemometer measurements for day and night during autumn 2013 at the INL test site. The sonic anemometer results reported are σ_v/U. The wind speed bins are 0–1, 0–2, 1–2, 2–4, 4–6, and >6 m s^{-1}. Error bars represent ±1 standard deviation. The PPG measurements are shown for reference.

done in previous decades. Figure 14 is a plot of the ratios of σ_y/σ_θ as a function of downwind distance for PSB1. Most PSB1 σ_y/σ_θ ratios fall near the upper limit of or above the range of values found in previous field experiments [cf. Fig. 4.21 in Slade (1968)]. An exception is test 2 whose ratios lie within the range of values in Slade's Fig. 4.21. Test 2 had the lowest U and was the most unstable of the four tests included in the analysis for σ_y (Fig. 9). Daytime results for PPG are included for reference. Similar to the observations in Figs. 7 and 8, there is a greater tendency for PSB1 ratios to exceed the bounds of the range with increasing downwind distance.

4. Discussion

The PSB1 σ_y values in Figs. 7 and 8 are systematically higher, respectively, than 1) the stability-class curves derived from the PPG data and other classical studies

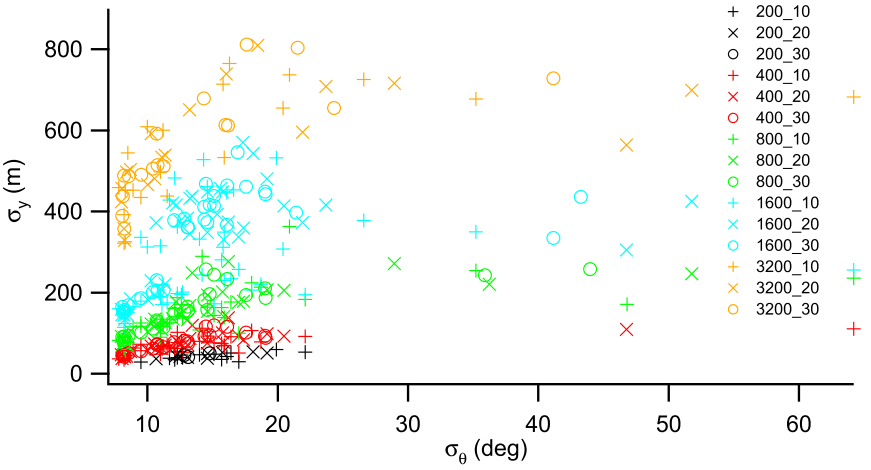

FIG. 13. Values of σ_y calculated by the second-moment method on nontruncated profiles for tests 2–5 as a function of σ_θ for different distances (the number in front of the annotation underscore; m) and averaging periods (the number following the underscore; min).

and 2) the semiempirical scheme used in the more modern AERMOD model. This is despite the turbulence levels during PSB1 and PPG showing similar behavior (Fig. 9). Possible explanations for these differences include the following:

1) There may be differences in site and/or meteorological conditions between PSB1 and previous studies that are not reflected in the σ_θ observations. This possibility is discussed below and will be the subject of future work.
2) There are differences in source configuration and plume sampling. PPG operated the tracer samplers continuously and set the plume averaging time by shutting off the source after 10 min. Thus, the PPG σ_y represent the integrated exposure to the passage of a discrete 10-min plume segment. In contrast, PSB1 used continuous releases of 2.5-h duration and set the averaging time by programming the samplers to fill bags for sequential 10-min intervals to obtain average concentrations.
3) The atmospheric tracers used in many of the older studies were not as strictly conservative as SF_6. For example, the SO_2 tracer in PPG was more prone to loss by deposition and reaction than is SF_6.
4) The P-G curves assume a sample averaging period of 3 min and a z_0 of 3 cm (Pasquill 1976).
5) Possible differences may arise from the method used for determining stability classification. That is, different methods could determine different stability

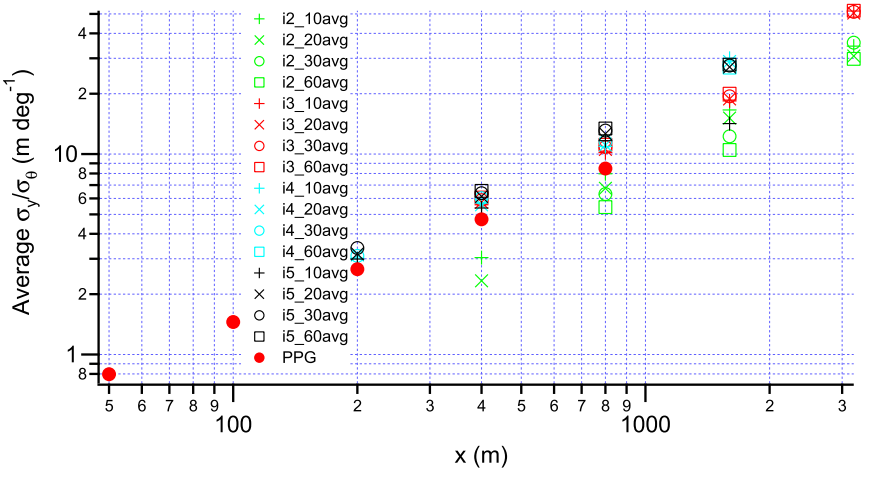

FIG. 14. Average ratios of σ_y/σ_θ for different averaging periods (“##avg”) as a function of downwind distance for tests 2–5 (“i2–i5”). The average ratios of σ_y/σ_θ from PPG are shown for reference.

categories as a result of the meteorological criteria used. For example, it was found that the SRDT and σ_θ methods often provided much different stability classifications during PSB1. On the other hand, the use of the SRDT alternative would have further exacerbated the differences in σ_y during PSB1.

6) There are differences in the assumed magnitudes of σ_θ used in different P-G methods for each stability category.

With regard to explanation 4, Pasquill (1976) and Hanna et al. (1977) point out that σ_y is a function of sample averaging time that should be accounted for. However, the results of PSB1 suggest that there is only a weak dependence for sample averaging periods ranging from 10 to 60 min. Furthermore, on the basis of the fast-response data, much of the plume variation was probably on time scales of 12–15 min or less.

With regard to explanation 2, Prairie Grass investigated the dispersion of 10-min plume segments rather than a true continuous plume. There was less chance for plume meander and turbulence to shred the segment in the time available, leaving a greater chance for the tracer to cross an arc at a specified distance as a more or less coherent cloud. In contrast, sampling during PSB1 used successive 10-min sampling intervals within a plume released continuously over more than 2 h. Each fixed 10-min sampling period had greater potential to be affected by plume segments with release durations of greater than 10 min. Portions of the tracer plume could have been pulled away from the main plume by turbulence, redirected by plume meander, and slowed down or sped up with respect to the main plume because of turbulence. This would more likely result in tracer-bearing parcels with more complex and different histories arriving at a specified arc distance within a given 10-min sampling period. The PPG parcels would be likely to have had histories that were less complex. These differences would tend to produce observed plume spreads for a given 10-min sampling period in PSB1 that were greater than the plume spreads during PPG, and they may in part account for the weakened effect of averaging time in PSB1.

Explanation 1 raises some questions and suggests avenues for further research. Are there peculiarities to the INL site that make it atypical, resulting in enhanced turbulence and plume spread? The results shown in Figs. 9 and 12 find little or no evidence that the observed daytime differences in σ_y between PSB1 and PPG can be attributed to INL site characteristics. The results of PSB1 suggest that stability-class schemes used to determine σ_y are, at a minimum, not universally applicable to all open, flat-terrain sites. How appropriate are the values of σ_θ used for the classification into the stability categories in existing P-G schemes (explanation 5 above)? Are σ_θ larger than is commonly recognized, especially at night? Daytime and nighttime discrepancies in σ_θ between PPG and those measured by modern meteorological instrumentation at the INL and at numerous other sites will be fully developed in a paper to follow.

Parts of the analysis drew upon Gaussian plume models that utilized stability-class methods that are based on results from the old tracer field studies for parameterization. Although their optimal use is restricted to situations that feature shorter-range dispersion, stationarity, and minimal terrain complexity, these models are preferred in some regulatory applications for being computationally fast and relatively easy to parameterize and configure, and they provide consistency with well-understood limitations. There has been an evolution in recent years toward the use of more-sophisticated dispersion models that use some form of Taylor's equation and PBL theory for the estimation of turbulence and model parameterization [e.g., the Hybrid Single-Particle Lagrangian Integrated Trajectory Model (HYSPLIT; Draxler and Hess 1997, 1998), RLINE (Snyder et al. 2013), and AERMOD (Cimorelli et al. 2004)]. Like the older stability-class models, however, these PBL models have also directly or indirectly drawn upon the old tracer studies for the setting of some parameters and/or for validation. The results of PSB1 raise questions about the parameterization and validation of any model that is based upon classical field studies such as PPG.

5. Conclusions

Project Sagebrush was started with the intent to re-evaluate results from the classical field experiments in short-range plume dispersion using newer technologies available for measuring both turbulence levels and tracer concentrations. Six key results from PSB1 were found:

1) Horizontal plume spread, as given through the values of σ_y, tended to be larger than that measured in previous field studies. As a result, the PSB1 σ_y values are larger than those predicted by both older modeling schemes, which are based on stability class, and the newer AERMOD scheme, which still retains empirical parameters that are derived from the classical tracer studies. Up to ~400-m distance downwind, the discrepancies in σ_y between PSB1, PPG, and the estimates determined by models developed from prior field studies were relatively minimal. As downwind distance increased, however, the discrepancies increased, with PSB1 σ_y becoming

larger by approximately a factor of 2. The PSB1 ratio of σ_y/σ_θ showed similar trend lines relative to prior field studies, but the ratios tend to fall near the upper limit or above the range of values found in previous field experiments.

2) One difference that may partly explain the larger values of σ_y in PSB1 is related to the source configuration. In PPG, the samplers ran continuously while the 10-min concentration averaging time was set by shutting off the source after 10 min. In PSB1, tracer was released continuously over more than 2 h while the 10-min averaging time was set by filling sequential bags over 10-min intervals. The latter configuration provides more opportunity for larger-scale eddies to affect the dispersion.
3) The PSB1 plume cross sections from a long-duration continuous source tended to exhibit a more non-Gaussian character than the PPG 10-min plume segments.
4) The evidence suggests that σ_y becomes independent of σ_θ for σ_θ greater than ~18°, which may be related to the failure of small-angle and slender-plume approximations.
5) The poor comparison between the observations of σ_y in PSB1 and those that were measured during PPG and predicted by the stability-class schemes, calls into question the continued usage of those schemes. However, the analysis suggests that newer models such as AERMOD may also need to be re-evaluated because of their reliance on the classical studies to set certain empirical parameters in their dispersion schemes.
6) The values of σ_θ measured during PPG are likely to be unrealistically low, especially at nighttime in low wind speed conditions. Any continued usage of stability-class dispersion models should be aware of this since PPG was an important contributor to their formulation.

Acknowledgments. We thank the staff from ARLFRD and a volunteer who participated in the field study (Shane Beard, Tom Strong, Jason Rich, Brad Reese, Roger Carter, Donna Davis, and Cherie Clawson). The authors thank Julia Flaherty for assistance with developing the second-moment algorithm. Funding for ARLFRD for this work was provided in part by NOAA, and the WSU participation was partly supported by the National Science Foundation Division of Atmospheric and Geospace Sciences under Grant 1112938.

REFERENCES

Arya, S. P., 1999: *Air Pollution Meteorology and Dispersion.* Oxford University Press, 310 pp.

Barad, M. L., Ed., 1958a: Project Prairie Grass, a field program in diffusion: Vol. I of Geophysical Research Papers 59. Air Force Cambridge Research Center Rep. AFCRC-TR-58-235(I), 280 pp. [Available online at http://www.jsirwin.com/PGrassVolumeI.pdf.]

——, 1958b: Project Prairie Grass, a field program in diffusion: Vol. II of Geophysical Research Papers 59. Air Force Cambridge Research Center Rep. AFCRC-TR-58-235(II), 209 pp. [Available online at http://www.jsirwin.com/PGrassVolumeII.pdf.]

Briggs, G. A., 1974: Diffusion estimation for small emissions. In Environmental Research Laboratories, Air Resources Laboratory, Atmosphere Turbulence and Diffusion Laboratory 1973 Annual Report. U.S. Atomic Energy Commission Rep. ATDL-106, 59 pp. [Available online at http://www.osti.gov/scitech/servlets/purl/5118833.]

Carruthers, D. J., R. J. Holroyd, J. C. R. Hunt, W. S. Weng, A. G. Robins, D. D. Apsley, D. J. Thompson, and F. B. Smith, 1994: UK-ADMS: A new approach to modelling dispersion in the earth's atmospheric boundary layer. *J. Wind Eng. Ind. Aerodyn.*, **52**, 139–153, doi:10.1016/0167-6105(94)90044-2.

Cimorelli, A. J., and Coauthors, 2004: AERMOD: Description of model formulation. U.S. Environmental Protection Agency Rep. EPA-454/R-03-004, 91 pp. [Available online at https://www3.epa.gov/scram001/7thconf/aermod/aermod_mfd.pdf.]

Clawson, K. L., R. M. Eckman, N. F. Hukari, J. D. Rich, and N. R. Ricks, 2007: Climatography of the Idaho National Laboratory 3rd edition. NOAA Tech. Memo. OAR ARL-259, 254 pp. [Available online at http://niwc.noaa.inel.gov/climate/INL_Climate_3rdEdition.pdf.]

Cramer, H. E., G. M. DeSanto, R. K. Dumbauld, P. Morgenstern, and R. N. Swanson, 1964: Meteorological prediction techniques and data system. Geophysical Corporation of America Rep. GCA-64-3-G, 252 pp.

Draxler, R. R., and G. D. Hess, 1997: Description of the HYSPLIT_4 Modeling System. NOAA Tech. Memo. ERL ARL-224, 24 pp. [Available online at http://www.arl.noaa.gov/documents/reports/arl-224.pdf.]

——, and ——, 1998: An overview of the HYSPLIT_4 modelling system for trajectories, dispersion, and deposition. *Aust. Meteor. Mag.*, **47**, 295–308. [Available online at http://www.bom.gov.au/amm/docs/1998/draxler.pdf.]

Eckman, R. M., 1994: Re-examination of empirically derived formulas for horizontal diffusion from surface sources. *Atmos. Environ.*, **28**, 265–272, doi:10.1016/1352-2310(94)90101-5.

EPA, 2000: Meteorological monitoring guidance for regulatory modeling applications. U.S. Environmental Protection Agency Rep. EPA-454/R-99-005, 171 pp. [Available online at https://www3.epa.gov/scram001/guidance/met/mmgrma.pdf.]

Finn, D., K. L. Clawson, R. G. Carter, J. D. Rich, R. M. Eckman, S. G. Perry, V. Isakov, and D. K. Heist, 2010: Tracer studies to characterize the effects of roadside noise barriers on near-road pollutant dispersion under varying atmospheric stability conditions. *Atmos. Environ.*, **44**, 204–214, doi:10.1016/j.atmosenv.2009.10.012.

——, and Coauthors, 2015: Project Sagebrush phase 1. NOAA Tech. Memo. OAR ARL-268, 338 pp. [Available online at http://www.arl.noaa.gov/documents/reports/ARL%20TM-268.pdf.]

Fuquay, J. J., C. L. Simpson, and W. T. Hinds, 1964: Prediction of environmental exposures from sources near the ground based on Hanford experimental data. *J. Appl. Meteor.*, **3**, 761–770, doi:10.1175/1520-0450(1964)003<0761:POEEFS>2.0.CO;2.

Garodz, L. J., and K. L. Clawson, 1991: Vortex characteristics of C5A/B, C141B, and C130E aircraft applicable to ATC terminal flight operations, tower fly-by data. NOAA Tech. Memo. ERL ARL-190, 250 pp. [Available online at http://www.arl.noaa.gov/documents/reports/ARL-190.pdf.]

——, and ——, 1993a: Vortex wake characteristics of B757-200 and B767-200 aircraft using the tower fly-by technique: Volume 1. NOAA Tech. Memo. ERL ARL-199, 160 pp. [Available online at http://www.arl.noaa.gov/documents/reports/ARL-199v1.pdf.]

——, and ——, 1993b: Vortex wake characteristics of B757-200 and B767-200 aircraft using the tower fly-by technique: Volume 2. Appendices. NOAA Tech. Memo. ERL ARL-199, 572 pp. [Available online at http://www.arl.noaa.gov/documents/reports/ARL-199v2.pdf.]

Gifford, F. A., 1961: Use of routine meteorological observations for estimating atmospheric dispersion. *Nucl. Safety*, **2**, 47–51.

——, 1976: Turbulent diffusion-typing schemes: A review. *Nucl. Safety*, **17**, 68–86.

Hanna, S. R., G. A. Briggs, J. Deardorff, B. A. Egan, F. A. Gifford, and F. Pasquill, 1977: AMS workshop on stability classification schemes and sigma curves—Summary and recommendations. *Bull. Amer. Meteor. Soc.*, **58**, 1305–1309.

Haugen, D. A., and J. J. Fuquay, Eds., 1963: The Ocean Breeze and Dry Gulch Diffusion Programs, Volume I. Air Force Cambridge Research Laboratories Rep. AFCRL-63-791(I), 240 pp. [Available online at http://oai.dtic.mil/oai/oai?verb=getRecord&metadataPrefix=html&identifier=AD0428436.]

Homann, S. G., and F. Aluzzi, 2014: HotSpot Health Physics Codes, version 3.0: User's Guide. Lawrence Livermore National Laboratory National Atmospheric Release Advisory Center Rep. LLNL-SM-636474, 198 pp. [Available online at https://narac.llnl.gov/content/assets/docs/HotSpot-UserGuide-3-0.pdf.]

Islitzer, N. F., and R. K. Dumbauld, 1963: Atmospheric diffusion–deposition studies over flat terrain. *Int. J. Air Water Pollut.*, **7**, 999–1022.

Jones, R., W. Lehr, D. Simecek-Beatty, and R. M. Reynolds, 2013: ALOHA (Areal Locations of Hazardous Atmospheres) 5.4.4: Technical Documentation. NOAA Tech. Memo. NOS OR&R 43, 96 pp. [Available online at http://response.restoration.noaa.gov/sites/default/files/ALOHA_Tech_Doc.pdf.]

Martin, D. O., 1976: Comment on "The change of concentration standard deviations with distance." *J. Air Pollut. Control Assoc.*, **26**, 145–146, doi:10.1080/00022470.1976.10470238.

Pasquill, F., 1961: The estimation of the dispersion of windborne material. *Meteor. Mag.*, **90**, 33–49.

——, 1975: Some topics relating to modelling of dispersion in boundary layer. U.S. Environmental Protection Agency Rep. EPA-650/4-75-015, 69 pp. [Available online at http://nepis.epa.gov/Exe/ZyPDF.cgi/20015UTI.PDF?Dockey=20015UTI.PDF.]

——, 1976: Atmospheric dispersion parameters in Gaussian plume modeling, Part II: Possible requirements for change in the Turner workbook values. U.S. Environmental Protection Agency Rep. EPA-600/4-76-030b, 52 pp. [Available online at http://nepis.epa.gov/Exe/ZyPDF.cgi/2000HVA4.PDF?Dockey=2000HVA4.PDF.]

Sagendorf, J. F., and C. R. Dickson, 1974: Diffusion under low windspeed, inversion conditions. NOAA Tech. Memo. ERL ARL-52, 89 pp. [Available online at http://www.arl.noaa.gov/documents/reports/ARL-52.pdf.]

——, R. G. Carter, and K. L. Clawson, 2001: MDIFF transport and diffusion models. NOAA Tech. Memo. OAR ARL-238, 26 pp. [Available online at http://www.arl.noaa.gov/documents/reports/arl-238.pdf.]

Slade, D. H., Ed., 1968: Meteorology and Atomic Energy. U.S. Atomic Energy Commission Office of Information Services Rep. TID-24190, 445 pp. [Available online at https://www.orau.org/ptp/PTP%20Library/library/Subject/Meteorology/meteorology%20and%20atomic%20energy.pdf.]

Snyder, M. G., A. Venkatram, D. K. Heist, S. G. Perry, W. B. Petersen, and V. Isakov, 2013: RLINE: A line source dispersion model for near-surface releases. *Atmos. Environ.*, **77**, 748–756, doi:10.1016/j.atmosenv.2013.05.074.

Start, G. E., and L. L. Wendell, 1974: Regional effluent dispersion calculations considering spatial and temporal meteorological variations. NOAA Tech. Memo. ERL ARL-44, 63 pp. [Available online at http://www.arl.noaa.gov/documents/reports/ARL-44.PDF.]

——, J. F. Sagendorf, G. R. Ackermann, J. H. Cate, N. F. Hukari, and C. R. Dickson, 1984: Idaho Field Experiment 1981 volume 2: Measurement data. U.S. Nuclear Regulatory Commission Rep. NUREG/CR-3488 Vol. 2, 937 pp. [Available online at http://www.osti.gov/scitech/servlets/purl/6896818.]

Taylor, G. I., 1921: Diffusion by continuous movements. *Proc. London Math. Soc.*, **20**, 196–211. [Available online at http://mhd.ens.fr/IHP09/Young/Biblio/Taylor1921.pdf.]

Trinity Engineering Associates, 2013: CAP88-PC version 3.0 user guide. Trinity Engineering Associates Rep., 209 pp. [Available online at http://www.epa.gov/sites/production/files/2015-05/documents/V3userguide_020913.pdf.]

Turner, D. B., 1970: Workbook of atmospheric diffusion estimates. U.S. Environmental Protection Agency Office of Air Programs Pub. AP-26, 84 pp. [Available online at http://www.dot.ca.gov/newtech/researchreports/1969-1970/70-07.pdf.]

Venkatram, A., M. G. Snyder, D. K. Heist, S. G. Perry, W. B. Petersen, and V. Isakov, 2013: Re-formulation of plume spread for near-surface dispersion. *Atmos. Environ.*, **77**, 846–855, doi:10.1016/j.atmosenv.2013.05.073.

Willis, G. E., and N. Hukari, 1984: Laboratory modeling of buoyant stack emissions in the convective boundary layer. *Proc. Fourth Joint Conf. on Applications of Air Pollution Meteorology*, Portland, OR, Amer. Meteor. Soc., 24–25.

Yamartino, R. J., 1984: A comparison of several "single-pass" estimators of the standard deviation of wind direction. *J. Climate Appl. Meteor.*, **23**, 1362–1366, doi:10.1175/1520-0450(1984)023<1362:ACOSPE>2.0.CO;2.